Masoero E, Jennings HM, Ulm FJ, DelGado E, Manzano H, Pellenq RJM, Yip S.

Modelling cement at fundamental scales: From atoms to engineering strength and durability.

***In:* Bicanic, N; Mang, H; Meschke, G; de Borst, R (eds.)**

***Computational Modelling of Concrete Structures*.**

Boca Raton; London; New York; Leiden: CRC Press, 2014, pp.139-148.

Modelling cement at fundamental scales: from atoms to engineering strength and durability

E. Masoero & H.M. Jennings & F.-J. Ulm
Department of Civil and Environmental Engineering
Massachusetts Institute of Technology, Cambridge, Massachusetts 02139, USA

E. Del Gado
Department of Civil, Environmental and Geomatic Engineering
ETH Zurich, 8093 Zurich, Switzerland

H. Manzano
Department of Physical Chemistry
UPV/EHU Barrio Sarriena s/n, 48940 Leioa, Bizkaia, Spain

R.J.-M. Pellenq
Department of Civil and Environmental Engineering
Massachusetts Institute of Technology, Cambridge, Massachusetts 02139, USA
<MSE>2, joint CNRS/MIT lab
Massachusetts Institute of Technology, Cambridge, Massachusetts 02139, USA
CINAM, CNRS/AIX
Marseille University, Campus de Luminy, 13288 MArseille, France

S. Yip
Department of Nuclear Science and Engineering
Massachusetts Institute of Technology, Cambridge, Massachusetts 02139, USA

ABSTRACT: The mechanics and rheology of cement pastes are largely determined by the calcium-silicate-hydrate (C–S–H) gel, which is normally the main binding phase. The C–S–H gel is an amorphous material with a nanoscale pore network. Here we consider a model structure of the gel, where a continuous molecular model of non-porous C–S–H is combined with a colloidal model that incorporates the porosity of the gel. Numerical simulations predict mechanical properties and microscopic processes associated with yielding under shear. The proposed model can now be used to extract further properties and to contribute to a broader effort aimed at describing and engineering the multi-scale structure and mechanical behaviour of the cement paste. We finally discuss the opportunities offered by our model with respect to the scientific and technological challenges of modelling and controlling ageing and creep over long time scales.

1 INTRODUCTION

The strength of solid cement paste is governed by the properties of a number of crystalline and amorphous phases (Bullard et al. 2011). In ordinary cement pastes, a central role is played by calcium-silicate-hydrate (C-S-H), which forms a disordered, nanoporous, highly cohesive phase called "C–S–H gel" which glues together the different components. Many macroscopic properties are largely controlled by sub-micrometer features and processes in the C–S–H gel. At these scales, Jennings 2008 have suggested a discrete model based on aggregates of colloidal nanoparticles to interpret a number of experimental observations (Allen et al. 2007, Constantinides and Ulm 2007). The challenge lies now in moving from qualitative tools for interpreting measurements, to quantitative predictions that can guide the design of new cementitious materials. Multi-scale modelling and simulations can contribute greatly by identifying the mi-

croscopic mechanisms that control the development of structural features and mechanical properties during the precipitation and ageing of the C–S–H gel.

Here we describe a recent numerical implementation of the colloidal description of the C–S–H gel (Masoero et al. 2012). The model generates random aggregates of cohesive nanoparticles that represent the C–S–H gel structure at the (meso-)scale of 1 to 100 nm. Model structures are generated using a Monte Carlo space-filling algorithm to insert nanoparticles into an initially empty simulation box. The particles are polydisperse in size and interact via a generalized size-dependent Lennard-Jones potential, parametrized to reproduce the mechanical behavior of C–S–H at the molecular scale (< 10 nm) as obtained from atomistic simulations. We show that the experimentally observed heterogeneities of local density in the C–S–H gel can be associated with a spatial variety of polydispersity of the nanoparticle aggregates. We then compute elastic properties and inelastic deformations at different packing densities. The calculated elastic moduli are in the same range as those measured with nano-indentation experiments. Irreversible deformations under finite shear strain are probed, and suggest possible mechanisms of irreversible deformation and of transition from elastic response to yielding. Finally, we discuss how this approach can contribute to the multi-scale description of cement paste and to investigate slow processes of creep and ageing.

2 MODEL CONSTRUCTION: FROM THE MOLECULAR TO THE MESOPOROUS STRUCTURE OF THE C–S–H GEL

2.1 *Bottom-up definition of C–S–H nanoparticles, starting from the molecular structure*

There is general agreement that the molecular structure of the C–S–H (indicatively below 5 nm) at room temperature can be regarded as an imperfect version of crystalline calcium-silicate-hydrates, in particular torbermorite and jennite (Taylor 1986, Cong and Kirkpatrick 1996, Richardson 1999, Richardson 2008, Pellenq et al. 2009). The molecular structures of the crystalline forms consist in an ordered stack of calcium oxide and water layer, ribbed by silica chains. Experiments on the C–S–H confirm a reminiscence of such layered structures. On the other hand, a significant amount of disorder is also present and is attributed to the excess of calcium relative to silicon, compared to the crystalline forms (the average calcium to silicon ratio C/S in the C–S–H is normally around 1.7, while in the crystalline phases is much lower ≈ 1). The high C/S ratio is due to the abundance of calcium in the ionic solution from which the C–S–H precipitates: a solution produced by mixing water and tricalcium silicate, a typical component of unhydated cement grains, would contain approximately 3 moles of calcium for each mole of silicon.

At the larger scale between 1 and 100 nm, water sorption (Powers 1958), small angle neutron scattering (SANS) (Allen et al. 2007), and nuclear magnetic resonance (NMR) experiments (Muller et al. 2013), they all indicate the presence of a network of mesopores (following the IUPAC definition, the mesopores are pores with diameter between 2 and 50 nm). Combining the pictures of a layered molecular structure and the presence of larger mesopores, led to two main models of the C–S–H gel at the sub-micrometer scale. The model from Feldman and Sereda 1968describes the C–S–H gel as the results of calcium-silicate layers that grow in the solution and that wrinkle while growing. Such wrinkling would be caused by the molecular defects due to the high C/S ratio. The mesopores of the gel can be included in such a picture: they would be simply larger imperfections within the heterogeneous structure. On the other hand, the model by Feldman and Sereda 1968does not attribute an important role to the mesopores for what concerns the mechanical response of the gel. For example, the irreversible shrinkage that occurs when drying from saturation down to 50% relive humidity, according to Feldman and Sereda 1968, is due to the collapse and sliding of C–S–H layers, without the gel porosity being necessarily affected. By contrast Jennings 2000, in agreement with previous works from Powers, developed a colloidal model of the C–S–H gel that attributes the development of irreversible deformations at relative humidities above 20%, exclusively to the relative sliding of discrete nanoparticles (below 20% relative humidity, the C–S–H layers inside the nanoparticles collapse (Bonnaud et al. 2012)). Within this picture, the C–S–H gel can be represented as an aggregate of nanoparticles, but the existence of such a nanoparticulate structure lacks of a strong, direct experimental proof (despite a number of experiments, e.g. instrumented nanoindentation and SANS, have been interpreted using this assumption). The debate is still ongoing, on what model is most appropriate and on whether the two can be reconciled to some extent (Jennings et al. 2008).

In this work, we use a recent numerical implementation of the colloidal model developed by some of us (Masoero et al. 2012). In this model, the structure and the mechanical properties of the system are controlled by strong cohesive interactions between the nanoparticles. An important novel feature is that, although the model is based on a discrete description of the gel, our strategy to translate information from the molecular scale to the nanoparticles is such that it released the hypothesis that the nanoparticles are well-defined, distinguished entities. Specifically, the interactions between nanoparticles that we have implemented were parametrized to reproduce the cohesion of a continuous molecular structure of C–S–H, without any assumption regarding the presence of a physical interface between nanoparticles. In other

words, in the elastic regime we have assumed that the interaction between two nanoparticles is exactly the same as the bulk behaviour inside the nanoparticles themselves, hence reducing the distinction between bulk and and interface to a mere arbitrary choice of discretization. Such implementation of the colloidal model can therefore also be seen as a discretization of a continuous "foamy" structure, analogously to how macroscopic heterogeneous materials and even buildings are modelled in the framework of the Discrete Element Method (Masoero et al. 2010).

The discrete representation of a continuum, nevertheless, comes with the price of artificially establishing preferential sites for local yielding, failure, and large deformations in general. This is where our model departs significantly from the view of Feldman and Sereda 1968, in favour of the colloidal description. In fact, we are assuming that the preferential sites for large deformations correspond to the interfaces between particles in our model. This assumption is supported by recent atomistic simulations (Pellenq et al. 2009) of the C–S–H (without mesopores) that do predict the presence of such preferential sites due to heterogeneities in the density at high C/S ratios. Atomistic simulations have also shown that these lower-density regions, possibly corresponding to thicker-than-average layers of water,

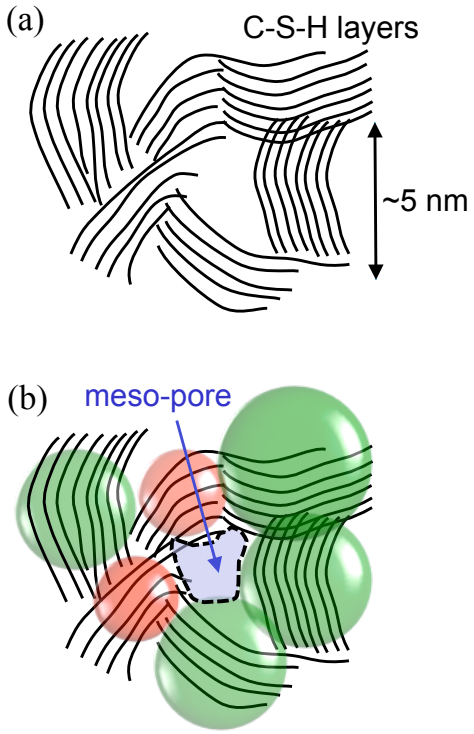

Figure 1: (a) Representation of the C–S–H gel structure, seen as a disordered assembly of layers at the molecular scale. (c) Colloidal representation obtained associating the interfaces between particles to defective regions of the molecular structure. With this discretization step and using (elastic) interaction potentials between the particles, we are effectively assuming that all inelastic deformations must occur at the interface between particles. For consistency with the rest of this manuscript, we have used the red colour to indicate small particles and the green colour for the large ones.

are where large displacements and irreversible deformations tend to concentrate when a shear strain is applied to a *continuous* molecular structure of C–S–H (Pellenq et al. 2009, Manzano et al. 2013, Manzano et al. 2013). Our interpretation is that the distribution of such "weak spots" in the molecular structure of the C–S–H controls the characteristic length of ≈ 5 nm that has been traditionally associated with the size of nanoparticles (Allen et al. 2007). This mechanistic definition of an interface between nanoparticles enables an efficient upscaling via discrete description of the C–S–H gel at scales between 1 and 100 nm.

2.2 *Size-dependent cohesive interactions*

In multiscale modelling, the interaction potentials between elements (or the constitutive laws) at a given scale must capture a set of properties that originate from the collective response at the scale below. Capturing all the details of the collective response at the lower scale would require extremely complex potentials, in principle with the same number of parameters as the number of degrees of freedom involved at the lower scale. On the other hand, many effects are averaged out in a complex system response, which already reduces the number of parameter needed. Furthermore, it is often convenient to decide what property one wants to describe at the larger scale, and then choose the minimum number of parameters to be inherited from the lower scale. This procedure is for example common when effective potentials for atomistic simulations are parametrized to reproduce a set of behaviours of few atoms that can be computed ab initio using quantum mechanics. Following this logics, we have chosen (Masoero et al. 2014) one of the possible functional forms of the effective interaction potential between two C–S–H nanoparticle, such that it allows describing a complex system with elastic response at low deformations and yielding and failure under large strain. The potential parameters are defined in such a way that it captures the elastic modulus $Y = 63.6$ GPa and the strain at rupture of the C–S–H obtained from atomistic simulations (Manzano et al. 2012, Manzano et al. 2013). The atomistic simulations indicate a strain rupture under shear $\gamma_u \approx 10\%$ which we convert into an equivalent uniaxial tensile strain at rupture $\varepsilon_u = (\sqrt{\gamma_u^2 + 2\gamma_u + 2} - \sqrt{2})/\sqrt{2} = 5.12\%$ following the geometric scheme in Fig. 2(a).

We employ the following single-well pairwise interaction potential:

$$U_{ij}\left(r_{ij}\right) = 4\,\varepsilon\left(\sigma_i, \sigma_j\right)\left[\left(\frac{\bar{\sigma}_{ij}}{r_{ij}}\right)^{2\alpha} - \left(\frac{\bar{\sigma}_{ij}}{r_{ij}}\right)^{\alpha}\right] . \quad (1)$$

r_{ij} is the inter-particle distance, ε is the well depth between two particles with different size σ_i and σ_j, α controls how narrow the potential well is, and $\bar{\sigma}_{ij} = (\sigma_i + \sigma_j)/2$. This potential has two salient features. First it admits of size polydispersity, i.e. the particles

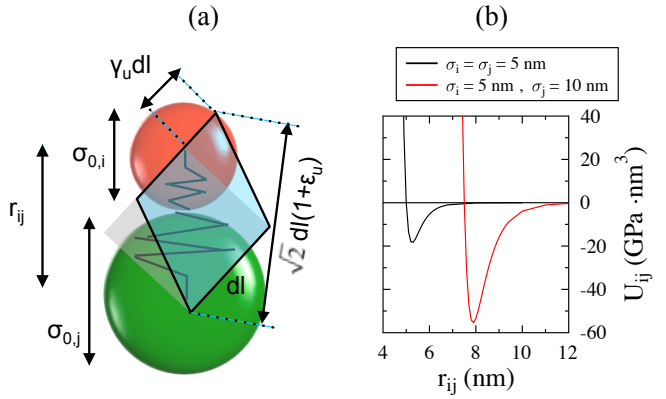

Figure 2: (a) Two interacting particles with different size, and cohesion modelled locally by springs. The geometric scheme to convert the shear strain at rupture at the molecular scale γ_u into an equivalent tensile strain at rupture ε_u is also shown. (c) Interaction potential between two particles with same size (in black) or different sizes (in red).

can have different diameters. Second, it implies that a particles cannot transfer shear forces to the others. In support to this second simplifying assumption, atomistic simulations predict that the shear strength of the C–S–H decreases remarkably in presence of regions with lower density, which we associate to the interfaces between particles in our model (Pellenq et al. 2009, Manzano et al. 2013).

The two parameters of the potential in Eq. 1, α and ε, are determined referring to ε_u and Y at the molecular scale. These are strength and elastic properties, which translate into first and second derivatives of the interaction potential. The tensile force is:

$$\frac{dU_{ij}\left(r_{ij}\right)}{dr_{ij}} = 4\,\frac{\varepsilon\left(\sigma_i,\sigma_j\right)}{\bar{\sigma}_{ij}}\left[2\alpha\left(\frac{\bar{\sigma}_{ij}}{r_{ij}}\right)^{2\alpha+1} - \alpha\left(\frac{\bar{\sigma}_{ij}}{r_{ij}}\right)^{\alpha+1}\right] \quad . \tag{2}$$

which becomes null when:

$$\frac{dU_{ij}\left(r_m\right)}{dr_{ij}} = 0 \quad \rightarrow \quad r_m = \sqrt[\alpha]{2}\,\bar{\sigma}_{ij} \quad . \tag{3}$$

Based on this we define the diameter of the ith particle $\sigma_0 = \sqrt[\alpha]{2}\sigma_i$. The maximum tensile force is at interparticle distance $r_{ij} = r_u$, for which the curvature of the potential is null. From:

$$\frac{d^2U_{ij}\left(r_{ij}\right)}{dr_{ij}^2} = 4\,\frac{\varepsilon\left(\sigma_i,\sigma_j\right)}{\bar{\sigma}_{ij}^2}\left[\left(4\alpha^2+2\alpha\right)\left(\frac{\bar{\sigma}_{ij}}{r_{ij}}\right)^{2\alpha+2} - \left(\alpha^2+\alpha\right)\left(\frac{\bar{\sigma}_{ij}}{r_{ij}}\right)^{\alpha+2}\right] \quad , \tag{4}$$

we obtain:

$$\frac{d^2U_{ij}\left(r_u\right)}{dr_{ij}^2} = 0 \quad \rightarrow \quad r_u = \sqrt[\alpha]{\frac{4\alpha+2}{\alpha+1}}\,\bar{\sigma}_{ij} \quad . \tag{5}$$

The strain at maximum tensile force is therefore:

$$\varepsilon_u = \frac{r_u - r_m}{r_m} = \frac{\sqrt[\alpha]{\frac{4\alpha+2}{\alpha+1}} + \sqrt[\alpha]{2}}{\sqrt[\alpha]{2}} \quad . \tag{6}$$

$\alpha = 14$ in Eq. 6 provides $\varepsilon_u = 4.82\%$ which we consider as a good approximation of $\varepsilon_u = 5.12\%$ that we obtained for C-S-H at molecular scale. In order to capture the Young modulus Y at the molecular scale with Eq. 1 we assume that at local equilibrium $r_{ij} = r_m$ the stiffness of our effective interaction potential, viz. the second derivative in Eq. 4, equals the stiffness of the springs in series in Fig. 2(a). The springs have length at rest $1/2\;\sigma_{0,i} = 1/2\;\sqrt[14]{2}\;\sigma_i$ and $1/2\;\sqrt[14]{2}\;\sigma_j$. In the harmonic approximation, treating the springs as De Saint Venant solids with cross sections $\pi(1/2\;\sqrt[14]{2}\;\sigma_i)^2$ and $\pi(1/2\;\sqrt[14]{2}\;\sigma_j)^2$, the stiffness of the spring system is:

$$k_{spr} = \frac{1}{\frac{1/2\;\sqrt[14]{2}\;\sigma_i}{Y\pi(1/2\;\sqrt[14]{2}\;\sigma_i)^2} + \frac{1/2\;\sqrt[14]{2}\;\sigma_j}{Y\pi(1/2\;\sqrt[14]{2}\;\sigma_j)^2}} \tag{7}$$

$$= \frac{Y\pi\sqrt[14]{2}}{2}\frac{\sigma_i\sigma_j}{\sigma_i+\sigma_j} = \frac{1}{4}\pi Y\;\sqrt[14]{2}\bar{\sigma}_{ij}\beta_{ij}\left(\sigma_i,\sigma_j\right) \quad .$$

$\beta_{ij} = \sigma_i\sigma_j/\bar{\sigma}_{ij}^2$ is a factor that emerges from the serial arrangement in Fig. 2(a) and causes the interaction between two particles with very different size be controlled by the smallest one in the pair. Equating k_{spr} with the curvature of our interaction potential when $r_{ij} = r_m$ yields (Eqs. 7, 4, 3, and $\alpha = 14$) :

$$\varepsilon\left(\sigma_i,\sigma_j\right) = 0.002324\,Y\beta_{ij}\left(\sigma_i,\sigma_j\right)\bar{\sigma}_{ij}^3 \quad . \tag{8}$$

When $\beta = 1$, the same expression of ε used in Masoero et al. 2012 is recovered.

We have determined (in Eq. 6) that the strain at tensile rupture at the molecular scale controls the narrowness of the interaction potential in Eq. 1 via the factor α. Furthermore, Eq. 8 shows that the energy scale ε is related to the Young modulus Y at the molecular scale. Eq. 8 also shows that ε scales as $\bar{\sigma}_{ij}^3$, i.e. large particles stick together more strongly than small ones (see Fig. 2(b)). Another implication is that, if one considers two interacting particles with same size $\sigma_i = \sigma_j \rightarrow \beta_{ij} = 1$, the unit pressure $\varepsilon\left(\bar{\sigma}_{ij}\right)/\bar{\sigma}_{ij}^3 = 0.1478$ GPa is a constant. As a consequence all mechanical quantities with dimension of force per unit area become scale-invariant, for example the specific energy, the pressure, the strength, and the elastic moduli. For particles with typical diameter of 5 nm (Allen et al. 2007) and $Y = 63.6$ GPa, the cohesive energy provided by Eq. 8 is $\varepsilon = 115.3$ eV. Although this value seems very high from a molecular perspective, one must not forget that interactions between nanoparticles involve hundreds of atoms, and that here we are implying the presence of strong bonds between

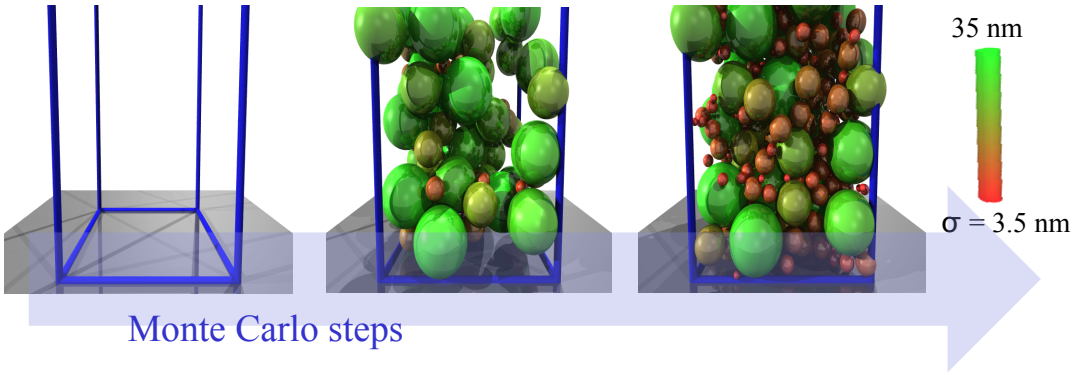

Figure 3: Snapshots from a simulation to generate a model C-S-H structure extracting particles from a reservoir with poldispersity $\delta = 0.47$. The color code indicates the particle size that, in our model, is indicative also of the strength of cohesion. Due to space filling, as the simulation advances the small particles increase in number compared to the large ones.

atoms at the interface when parametrizing the interaction potential based on bulk properties of the C-S-H. The high energy scale leads to a very small dimensionless temperature $T^* = k_B T/\varepsilon(\bar{\sigma}_{ij})$, which is a measure of the importance of thermal fluctuations (k_B is the Boltzmann constant). For example for room temperature $T = 298$ K and $\bar{\sigma}_{ij} = 5$ nm, we obtain $T^* \approx 2.22 \times 10^{-4}$. Notwithstanding such small value, in all our simulations we record non-negligible fluctuations due to thermal effects, especially for the smallest particles because of the scaling $\varepsilon(\bar{\sigma}_{ij}) \propto \bar{\sigma}_{ij}^3$.

2.3 *Generating model colloidal structures of the C–S–H gel*

We generate model C-S-H gel sub-micron structures using a Monte Carlo space filling algorithm to minimize the interaction energy (Masoero et al. 2012). We consider an initially empty cubic simulation box of linear size L in contact with an infinite reservoir of C-S-H nanoparticles. The linear size σ of the particles in the reservoir follows a uniform distribution between a minimum σ_m and a maximum σ_M value. The standard deviation δ of this distribution in units of $1/2\,(\sigma_M + \sigma_m)$ defines the polydispersity. A particle size is randomly extracted from the reservoir and an insertion at random location in the simulation box is tried. The insertion is accepted with probability $P_{creat} = \exp(-\Delta U/k_B T)$, where k_B is the Boltzmann constant, $T = 298$ K is the room temperature, and ΔU is the difference in total interaction energy between the particles inside the box (see Eq. 1) caused by the trial insertion. We also allow for particle displacements within the box, trying $D_p N$ Metropolis Monte Carlo moves in the NVT ensemble after every trial insertion. N is the number of particles in the box, which increases with the simulation time, and D_p is an arbitrary "delay" parameter, qualitatively inverse to a precipitation rate. The algorithm proceeds until N approaches a constant maximum value, i.e. space is filled. A typical sequence of snapshots is shown in Fig. 3.

Our model structures of the C–S–H gel capture the presence of a disordered network of mesopores. The solid volume fraction, or packing fraction $\phi = \sum_i \pi/6\, \sigma_{0,i}^3/L^3$, refers to the particle diameter defined previously $\sigma_0 = \sqrt[14]{2}\sigma$. A better packing is achieved at high polydispersity (Masoero et al. 2012, Masoero et al. 2014), probably because the increase of degrees of freedom enables to better minimize the interaction energy by filling the space more efficiently. As space filling proceeds, inserting large particles becomes unlikely while smaller particles can still fit (see Fig. 3). This causes the final particle size distribution to differ significantly from the uniform distribution in the reservoir. The final particle size distribution are geometric (Masoero et al. 2012, Masoero et al. 2014), analogously to the optimal space-filling distributions of hard spheres in Brouwers 2006. The power law regime that characterizes the geometric distributions for a wide range of particle diameters may be related with the power law signals from experiments of small angle neutron scattering on the C-S-H gel (Allen et al. 2007, Brisard and Levitz 2013).

3 MECHANICAL PROPERTIES OF THE MODEL C–S–H GEL STRUCTURES

In this section we investigate the mechanical properties of the sub-micron model C-S-H structures obtained from the space-filling simulations. The structures at the end of the space filling turn out to be all under negative pressure, i.e. tensile virial (Frenkel and Smit 2001) normal stresses. The reason lies in the attractive part of the interaction potential that dominates the state of stress of our colloidal system (differently from what one would expect from a weakly attractive or a purely repulsive granular packing). These negative pressure can reach several hundreds of MPa's, and therefore we decide to impose more realistic ambient conditions by relaxing the system to zero stress via isotension isothermal NtT ensemble(Najafabadi and Yip 1983, Hill 1956). Due to the large unit pressure in our model (0.148 GPa), null dimensionless stresses are satisfactorily representative of ambient pressure. We prefer the NtT over the isobaric NPT

ensemble because relaxing all six stress components independently toward zero provides a reference configuration that is appropriate to any type of subsequent test conditions, e.g. volumetric or deviatoric.

3.1 *Elastic properties at zero stress*

The tensor of elasticity is computed keeping fixed the simulation box after equilibration to zero stress, and using the stress fluctuation method by Lutsko 1989. According to this method the 6×6 tensor of elasticity in Voigt notation [C] is decomposed into a configurational contribution related to the second derivatives of the potential in Eq. 1, and a stress fluctuation component that includes temperature. The tensors of elasticity for all our model C–S–H gel structures with different polydispersity, satisfy the conditions for isotropy to hold (Masoero et al. 2014). We can then employ the Voigt formulas to obtain the bulk and the shear moduli of linear elasticity K, G (see Nye 1985 and Masoero et al. 2014). Finally, the indentation modulus M can be computed as (Constantinides and Ulm 2007):

$$M = 4G\frac{3K+G}{3K+4G} \quad . \tag{9}$$

Fig. 4 relates the calculated indentation moduli with the packing fractions of the model structures. It also shows a comparison with experimental data for a white cement paste (Pellenq et al. 2009). The agreement is good both in terms of overall linear trend, and from a quantitative point of view.

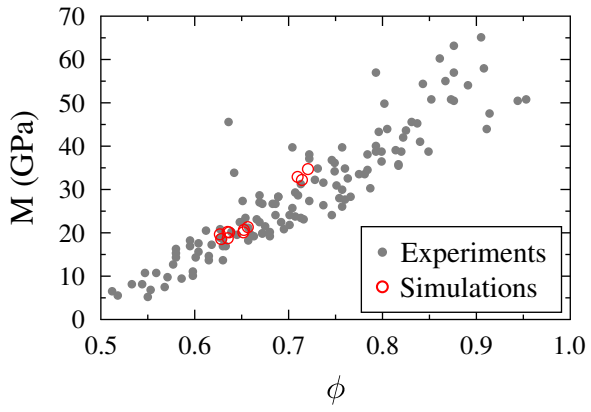

Figure 4: Indentation moduli vs. packing fraction. Results from our model (red triangles) and from the experimental study in ... (gray squares in the background).

3.2 *Shear stress-strain curves*

The model C-S-H configurations relaxed to zero stress are now subjected to a series of pure shear strain increments $\Delta\varepsilon_{xz} = \Delta\varepsilon_{zx} = \gamma/2$. After each increment, between 5×10^7 and 3×10^8 Monte Carlo trial displacements are performed to relax in the NhT ensemble, i.e. keeping the simulation box fixed. Fig. 5 shows the evolution of shear stress τ (in fact τ_{xz}) with γ. All curves start with a linear elastic regime, with elastic moduli that are consistent with those obtained from the stress tensors in Section 3.1. The linear elastic regime does not last long, and already at very low strain $\gamma < 0.03$ all the curves in Fig. 5 display at least one sudden drop of τ. After a drop of τ, the systems usually enter a new elastic regime of increase of τ, which gets interrupted again by the next drop. The slope of the linear regimes is the local shear modulus G, and it does not change significantly with γ (Masoero et al. 2014). By contrast, the amount and magnitude of shear drops increase with γ. In particular, we can observe an overall (including linear regimes and drops) increase of τ with γ for values of $\gamma \lesssim 0.1$. For values of $\gamma > 0.1$, the stress-strain curve oscillate around a constant value $\tau = \tau_y$, which indicates that the system has undergone yielding. τ_y increases significantly with the polydispersity δ. It is tempting to associate τ_y to the strength of the systems and to relate it to hardness measurements from nanoindentation (Constantinides and Ulm 2007). On the other hand, further analyses in (Masoero et al. 2014) show a significant build-up of pressure: negative at low polydispersity $\delta = 0$ and $\delta = 0.19$, and positive at high polydispersity $\delta = 0.38$. This is indicative of typical granular behaviours of compaction and dilation under shear. The observed coupling between the deviatoric (shear) and the hydrostatic (pressure) components of stress, prevents us from characterizing the strength of our systems only from the curves in Fig. 5. In fact a strength domain should be obtained in the Mohr-Coulomb framework, and a full set of simulations of failure under different combinations of shear stress and pressure would be required in order to do that.

As expected for systems that evolve towards yielding, the analyses in (Masoero et al. 2014) have shown that most of the stress drops in Fig. 5 are accompanied by the development of irreversible deformations.

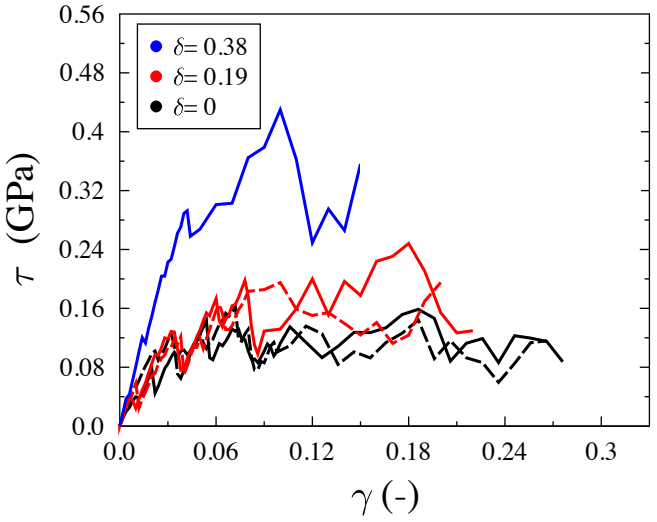

Figure 5: Pure shear load tests by Masoero et al. 2014, for single realizations of model C–S–H gel structures with different packing densities induced by different levels of allowed particle size polydipsersity δ.

In other words, if one picks a $\tau - \gamma$ point from one of the curves in Fig. 5 and performs a simulation to re-establish $\tau = 0$ by reducing γ, the result would be that $\tau = 0$ is reached already at a level of (residual or irreversible shear strain) $\gamma_p > 0$. It is also worth noting that the irreversible strain γ_p increases by discrete steps as γ is increased, and that this happens in correspondence of the stress drops. Usually, an increase of γ_p (and therefore a drop of τ too) is accompanied also by a change in residual energy U_0, i.e. the total interaction energy between the particles after relaxing the system from a generic $\tau - \gamma$ state back to $\tau = 0$. The results in (Masoero et al. 2014) also showed that γ_p increases weakly while $\gamma \lesssim 0.1$ and then ramps up more significantly and linearly for $\gamma \gtrsim 0.1$. This implies that the constitutive behaviour of the material can be approximately described as elasto-pastic.

Finally, a last result worth mentioning is the different contribution to the overall displacement field coming from particles with different size. In particular, we measured the non-affine part of the displacement of each particle (Masoero et al. 2014). The non-affine displacment is related to irreversible transformations. In fact, the average non-affine displacement of the particles in the systems displays a peak (compared to the average non-affine displacement within an elastic regime) when a stress drop takes place and the irreversible strain increases. We have observed that in our polydisperse systems, the smallest particles are those that display the greatest non-affine displacements during an irreversible event. The concentration of non-affine displacments in the small particles becomes particulary strong after yielding, when the large particles tend to move by affine convection only. This suggests that yielding can be associated with the unlocking of large particles, that are circumvented by the small ones and begin to operate as hard inclusions in a deformable matrix of smaller particles. This highlights a possible mechanistic explanation for yielding in polydisperse systems, and stimulates questions on how this mechanisms can be tuned in order to engineer the mechanical behaviour of the C–S–H gel under large deformations.

4 DISCUSSION: MULTI-SCALE DESCRIPTION IN SPACE AND TIME

We have developed a model for the C–S–H gel structure and mechanical behaviour at scales between 1 nm and 1 μm. A central ingredient of the model is the effective interaction potential between nanoparticles, which we have developed and parametrized referring to simulated structural features and mechanical properties at the smaller scale of the molecular structure of the C–S–H. This is a first example of crossing scales within the multi-scale description of cement paste. More recently, the effect of the solution chemistry on the interaction potential between the nanoparticles, and therefore on the resulting morphology and mechanical properties of the C–S–H gel, has also been considered (Ioannidou et al. 2014). Further studies in these directions are expected to ultimately provide modelling and simulation tools that can complement the experimental approaches for the design of new, more sustainable, cementitious materials.

One necessary next step is now to link the results of our model at the gel scales, with model at larger scales. For example, it is known that the packing density of the C–S–H gel (viz. the amount of mesopores) can have a significant effect on the hydration kinetics of the cement paste (Bishnoi and Scrivener 2009). A number of existing models of cement hydration tackle the problem at scales between 100 nm and 1 μm, using continuum-based theories like nucleation and growth (Thomas et al. 2011, Masoero, Thomas, & Jennings 2013). These continuum-based approaches rely upon a number of input parameters that can be computed, better understood, and possibly controlled and engineered, using our nanoparticle model at the scale below. While such goal seems reasonably at reach for what concerns the structural (e.g. multi-scale pore network) and short-term mechanical (e.g. elastic moduli and strength) descriptions, more serious issues are raised by slow evolution processes like precipitation, creep, and ageing.

The issue of time-scales originate from the fact that the dynamics of a system, i.e. the explicit integration of Newton's equations for its interacting elements, can normally be simulated only over time-scales of the order of $t_{max} \sim 10^8 t_c$. t_c is a characteristic time that is in the order of $\sim 0.01 c/\sigma$, where c is the speed of sound between two interacting elements, and σ is the typical equilibrium distance between the elements. The speed of sound can be estimated as $c = \sqrt{Y/\rho}$, where Y is the Young modulus and ρ is the density. At the scale of our C–S–H gel particles, $Y = 63.5$ GPa, $\rho = 2,650$ kg/m^3, and $\sigma \sim 5$ nm. This yields $t_{max} \sim 63$ μs. Macroscale simulations of the progressive collapse of buildings made of reinforced concrete can be performed using the Discrete Element Method, which is also based on Newton's equations of motion, like molecular dynamics at small scales. For reinforced concrete, $Y \sim 30$ GPa, $\rho \sim 2500$ kg/m^3, and $\sigma \sim 1$ m. Y and ρ being quite similar to those at the nanoscale of the C–S–H, the main effect on the time-scale accessible by dynamics simulation is the characteristic length-scale σ. The much larger σ of the reinforced concrete case, in fact, leads to maximum simulation times of the order of $t_{max} \sim 200$ s. Still, neither the t_{max} of our model C–S–H gels nor that of macroscale reinforced concrete, are comparable with the time scales involved in cement hydration (hours and days) and creep and ageing (years and centuries). Furthermore, strain rate effects can change qualitatively the material response at the fundamental scales (Fan, Osetskiy, Yip, & Yildiz

2013). This leads to the further issue that even the short-term mechanical response predicted by dynamic simulations at the fundamental scales, where strain rates are of the order of per-nanoseconds, may not be related to short-term deformation processes at the macro-scale, where strain rates could be of the order of per-milliseconds.

Kinetic approaches provide an alternate route to simulate the behaviour of materials across time-scales (Vineyard 1957, Kushima et al. 2009, Lau et al. 2009, Kushima et al. 2011, Mousseau et al. 2012, Yip and Short 2013). The main idea is that the system evolution is controlled by rare events that let the system hop from one local minimum in the potential energy landscape (state of local, generally metastable, equilibrium) to the next one. This transition of state is generally accompanied by a change of system-wide quantities, for example pressure, deformation, and potential energy. In order for the transition to occur, the system must overcome the barrier of potential energy that separates the initial and final local minima (activation energy). The time Δt that a system requires to hop an energy barrier ΔE during its thermal fluctuations, can be estimated from the Transition State Theory (TST):

$$\Delta t = \frac{1}{\nu_0} e^{\frac{\Delta E}{k_B T}} \quad , \tag{10}$$

where ν_0 is a characteristic frequency of vibration (of the order t_c^{-1}, where t_c is the characteristic time defined earlier in this Section), k_B is the Boltzmann constant, and T is the temperature in Kelvins. ΔE can be reduced via external actions, for example applying a stress that provides strain energy which raises the energy level of the system in the local minimum. There exists therefore a coupling between mechanical and thermal (Eq. 10) activation of transitions. Within this context, our modelling approach to the C–S–H gel can provide extremely valuable informations regarding the possible transitions and the associated energy levels of minima and barriers that the system encounters during its elasto-plastic deformation. In fact, the stress drops in Fig. 5are signatures of energy barrier hops induced by mechanical activation. There is a lot of promising ongoing work in this sense, for what concerns both C–S–H gel in cement and other materials systems (Masoero et al. 2013, Yip and Short 2013).

5 CONCLUSIONS

We have presented a polydisperse colloidal model of the C–S–H gel at length scales between 1 and 100 nm. The model is constructed based on an effective interaction potential between nanoparticles that has been developed starting from information gathered at the molecular scale. Our colloidal model can be interpreted as a discrete representation of a defective continuum where some mechanical properties in correspondence of the most defective regions (modelled as interfaces between nanoparticles) are comparable with the bulk properties of the less imperfect regions of the molecular structure. This is a picture that is also emerging from recent molecular models and simulations.

Our model predicts a range of C–S–H gel structures with packing densities and elastic properties that agree well with the results of instrumented nanoindation tests. We have also simulated the mechanical behaviour under large shear deformations, identifying a prevalent linear elastic response at small strain, followed by yielding occurring at higher strain levels. A more detailed analysis of the accumulation of irreversible deformations and associated non-affine displacements provides new insight on the mechanisms of deformation and failure of polydisperse, cohesive systems.

Finally, we have discussed the impact of our research on the multi-scale description of the cement paste. We have demonstrated that results from modelling at the molecular scale can be translated into inputs (the interaction potentials) that predict structural features and mechanical properties at the larger scale of the gel. A similar approach can now be applied for the next upscaling step to the micrometer scale, which is relevant for example to the problems of hydration and to combine the mechanical properties of the C–S–H gel with those of other hydration products. We have also discussed the challenge of the time-scale, i.e. understanding how mechanisms that occur at fundamental scales are relevant to the temporal evolution of the cement paste at the macroscale, for example with respect to creep and ageing. Combinations of Transition State Theory and direct simulations akin to those presented here, will likely offer new opportunities to better understand and engineer the slow chemo-mechanical behaviour of the cement paste.

REFERENCES

Allen, A. J., J. J. Thomas, & H. M. Jennings (2007). Composition and density of nanoscale calcium-silicate-hydrate in cement. *Nat. Mater. 6*, 311–316.

Bishnoi, S. & K. L. Scrivener (2009). Studying nucleation and growth kinetics of alite hydration using μic. *Cem. Concr. Res. 39*, 849–860.

Bonnaud, P., Q. Ji, B. Coasne, R.-M. Pellenq, & K. Van Vliet (2012). Thermodynamics of water confined in porous calcium-silicate-hydrates. *Langmuir 28*(31), 11422–11432.

Brisard, S. & P. Levitz (2013). Small-angle scattering of dense, polydisperse granular porous media: Computation free of size effects. *Physical Review E 87*(1), 013305.

Brouwers, H. (2006). Particle-size distribution and packing fraction of geometric random packings. *Physical review E 74*(3), 031309.

Bullard, J. W., H. M. Jennings, R. A. Livingston, A. Nonat, G. W. Scherer, J. S. Schweitzer, K. L. Scrivener, & J. J. Thomas (2011). Mechanisms of cement hydration. *Cem. Concr. Res. 41*, 1208–1223.

Cong, X. & R. J. Kirkpatrick (1996). ^{29}Si MAS NMR study of the structure of calcium silicate hydrate. *Advanced Cement Based Materials 3*(3), 144–156.

Constantinides, G. & F.-J. Ulm (2007). The nanogranular nature of C–S–H. *J. Mech. Phys. Solids 55*, 64–90.

Fan, Y., Y. N. Osetskiy, S. Yip, & B. Yildiz (2013). Mapping strain rate dependence of dislocation-defect interactions by atomistic simulations. *Proceedings of the National Academy of Sciences 110*(44), 17756–17761.

Feldman, R. F. & P. J. Sereda (1968). A model for hydrated portland cement paste as deduced from sorption-length change and mechanical properties. *Matériaux et Construction 1*(6), 509–520.

Frenkel, D. & B. Smit (2001). *Understanding molecular simulation: from algorithms to applications*. Access Online via Elsevier.

Hill, T. (1956). *Statistical Mechanics*. New York: McGraw-Hill.

Ioannidou, K., R. J.-M. Pellenq, & E. Del Gado (2014). Controlling local packing and growth in calcium–silicate–hydrate gels. *Soft Matter*.

Jennings, H. M. (2000). A model for the microstructure of calcium silicate hydrate in cement paste. *Cement and Concrete Research 30*(1), 101–116.

Jennings, H. M. (2008). Refinements to colloid model of csh in cement: Cm-ii. *Cement and Concrete Research 38*(3), 275–289.

Jennings, H. M., J. W. Bullard, J. J. Thomas, J. E. Andrade, J. J. Chen, & G. W. Scherer (2008). Characterization and modeling of pores and surfaces in cement paste. *Journal of Advanced Concrete Technology 6*(1), 5–29.

Kushima, A., J. Eapen, J. Li, S. Yip, & T. Zhu (2011). Time scale bridging in atomistic simulation of slow dynamics: viscous relaxation and defect activation. *The European Physical Journal B 82*(3-4), 271–293.

Kushima, A., X. Lin, J. Li, J. Eapen, J. C. Mauro, X. Qian, P. Diep, & S. Yip (2009). Computing the viscosity of supercooled liquids. *The Journal of chemical physics 130*, 224504.

Lau, T. T., A. Kushima, & S. Yip (2009). An atomistic method for slow structural deformations. In *IOP Conference Series: Materials Science and Engineering*, Volume 3, pp. 012002. IOP Publishing.

Lutsko, J. F. (1989). Generauzed expressions for the calculation of elastic constants by computer simulation. *J. Appl. Phys. 65*(8).

Manzano, H., E. Masoero, I. Lopez-Arbeloa, & H. Jennings (2013). Mechanical behaviour of ordered and disordered calcium silicate hydrates under shear strain studied by atomic scale simulations. In *Mechanics and Physics of Creep, Shrinkage, and Durability of Concrete@ sA Tribute to Zdenk P. Bazant*, pp. 86–97. ASCE.

Manzano, H., E. Masoero, I. Lopez Arbeloa, & H. M. Jennings (2013). Molecular modelling of shear deformations in ordered and disordered calcium silicate hydrates. *Soft Matter*, –.

Manzano, H., S. Moeini, F. Marinelli, A. C. Van Duin, F.-J. Ulm, & R. J.-M. Pellenq (2012). Confined water dissociation in microporous defective silicates: Mechanism, dipole distribution, and impact on substrate properties. *Journal of the American Chemical Society 134*(4), 2208–2215.

Masoero, E., E. Del Gado, R. J.-M. Pellenq, S. Yip, & F.-J. Ulm (2014). Nano-scale mechanics of colloidal c–s–h gels. *Soft Matter*.

Masoero, E., E. Del Gado, R.-M. Pellenq, F.-J. Ulm, & S. Yip (2012). Nanostructure and nanomechanics of cement: Polydisperse colloidal packing. *Physical review letters 109*(15), 155503.

Masoero, E., H. Manzano, E. Del Gado, R. Pellenq, F. Ulm, & S. Yip (2013). Kinetic simulation of the logarithmic creep of cement. In *Mechanics and Physics of Creep, Shrinkage, and Durability of Concrete@ sA Tribute to Zdenk P. Bazant*, pp. 166–173. ASCE.

Masoero, E., J. J. Thomas, & H. M. Jennings (2013). A reaction zone hypothesis for the effects of particle size and water-to-cement ratio on the early hydration kinetics of C_3S. *J. Am. Ceram. Soc*. In press.

Masoero, E., F. Wittel, H. Herrmann, & B. Chiaia (2010). Progressive collapse mechanisms of brittle and ductile framed structures. *Journal of engineering mechanics 136*(8), 987–995.

Mousseau, N., L. K. Béland, P. Brommer, J.-F. Joly, F. El-Mellouhi, E. Machado-Charry, M.-C. Marinica, & P. Pochet (2012). The activation-relaxation technique: Art nouveau and kinetic art. *Journal of Atomic, Molecular, and Optical Physics 2012*.

Muller, A., K. Scrivener, A. Gajewicz, & P. McDonald (2013). Use of bench-top nmr to measure the density, composition and desorption isotherm of csh in cement paste. *Microporous and Mesoporous Materials*.

Najafabadi, R. & S. Yip (1983). Observation of finite-temperature bain transformation (fcc bcc) in monte carlo simulation of iron. *Scripta metallurgica 17*(10), 1199–1204.

Nye, J. F. (1985). *Physical properties of crystals: their representation by tensors and matrices*. Oxford University Press.

Pellenq, R. J.-M., A. Kushima, R. Shahsavari, K. J. Van Vliet, M. J. Buehler, S. Yip, & F.-J. Ulm (2009). A realistic molecular model of cement hydrates. *Proceedings of the National Academy of Sciences 106*(38), 16102–16107.

Powers, T. C. (1958). Structure and physical properties of hardened portland cement paste. *Journal of the American Ceramic Society 41*(1), 1–6.

Richardson, I. (1999). The nature of csh in hardened cements. *Cement and Concrete Research 29*(8), 1131–1147.

Richardson, I. (2008). The calcium silicate hydrates. *Cement and Concrete Research 38*(2), 137–158.

Taylor, H. F. (1986). Proposed structure for calcium silicate hydrate gel. *Journal of the American Ceramic Society 69*(6), 464–467.

Thomas, J., J. Biernacki, J. Bullard, S. Bishnoi, J. Dolado, G. Scherer, & A. Luttge (2011). Modeling and simulation of cement hydration kinetics and microstructure development. *Cem. Concr. Res 41*, 1257–1278.

Vineyard, G. H. (1957). Frequency factors and isotope effects in solid state rate processes. *Journal of Physics and Chemistry of Solids 3*(1), 121–127.

Yip, S. & M. P. Short (2013). Multiscale materials modelling at the mesoscale. *Nature materials 12*(9), 774–777.